arXiv:1603.06248v1 [q-bio.NC] 20 Mar 2016

Gamma synchronization of the hippocampal spatial map—topological model

Edward Basso[1], Mamiko Arai[2] and Yuri Dabaghian[3,4*]

[1] *Department of Physics, Rice University, 6100 Main St. Houston, TX 77005 US*
[2]*Department of Mathematics, Tokyo Women's Christian University, 2-6-1 Zempukuji, Suginami-ku, Tokyo 167-8585, Japan*
[3]*Jan and Dan Duncan Neurological Research Institute, Baylor College of Medicine, Houston, TX 77030, USA*
[4]*Department of Computational and Applied Mathematics, Rice University, Houston, TX 77005, USA*
[*]*e-mail: dabaghia@bcm.edu*

(Dated: March 22, 2016)

The mammalian hippocampus plays a principal role in producing a cognitive map of space—an internalized representation of the animal's environment. The neuronal mechanisms producing this map depend primarily on the temporal structure of the hippocampal neurons' spiking activity, which is modulated by the oscillatory extracellular electrical field potential. In this paper, we discuss the integrative effect of the gamma rhythm, one of the principal components of these oscillations, on the ability of the place cell ensembles to encode a spatial map. Using methods of algebraic topology and statistical physics, we demonstrate that gamma-modulation of neuronal activity generates a synchronized spiking of dynamical cell assemblies, which enables learning a spatial map at faster timescales.

I. INTRODUCTION

The mammalian hippocampus plays a key role in spatial cognition. Place cells, the principal hippocampal neurons, manifest remarkable spatial specificity of spiking activity. They fire only in select locations in the environment. These locations are known as their respective place fields [1]. As a result, the place cells' spike trains contain information about the animal's current location [2], its future [3] and past [4] navigation routes, both in the wakeful state and even in sleep [5]. Moreover, damages to the hippocampal network produce impairments in spatial learning and difficulties in navigation planning [6, 7]. It is hence believed that the place cell ensembles encode an internalized "map" that serves as a basis of animal's spatial awareness [8, 9].

Motivation. An increasing amount of both direct [10–14] and indirect [15–19] experimental evidence suggests that this map is topological in nature, a rough-and-ready connectivity framework into which other brain regions integrate more detailed metrical information. A number of approaches have been deployed to understand the neuronal computations that could produce such a framework [20–29]. In particular, the approach proposed in [22–24] exploits the connection between the place fields covering an environment and the Alexandrov-Čech theorem, which points out the possibility of reconstructing the topology of a space X from the pattern of overlaps between regions that cover X. The fact that the place fields produce a dense cover of the environment suggests that the pattern of overlaps between them contains the information required to represent the environment's topology, which may hold the key to the way in which the hippocampus encodes its topological map of s pace. This observation is taken further by noticing that the domains where several place fields overlap are precisely the ones where the corresponding place cells cofire. In other words, the information about the overlap of place fields is represented via the place cell coactivity, which suggests that the Alexandrov-Čech construction can be carried out not only via geometric pattern of the place field overlaps, but also through the analysis of the place cell coactivities.

Topological model. The details of the topological model of the hippocampal map are discussed in [23, 24], but in brief, the idea is to represent the combinations of coactive place cells (c_1, c_2, ..., c_p) as multi-dimensional polyhedra—the "coactivity simplexes," $\sigma = [c_1, c_2, ..., c_p]$ (see Methods). Together, these coactivity simplexes form a simplicial "coactivity complex" $\mathcal{T}_\sigma$. In his construction, the individual cell groups, just like simplexes, provide local information about the space; joined together into a simplicial complex, modeling a neuronal ensemble, they represent space as whole. Numerical simulations demonstrate that $\mathcal{T}_\sigma$ captures the topological structure of the environment and serves as a schematic representation of the hippocampal map [23, 29]. For example, the sequences of place cell combinations ignited along the paths traversed by the animal are represented in $\mathcal{T}_\sigma$ by chains of coactivity simplexes—the simplicial paths [30, 31]. A non-contractible simplicial path may represent a navigational path γ that encircles a physical obstacle, whereas topologically trivial simplicial paths correspond to contractible routes in the physical space (Figure 1A,B).

The complex $\mathcal{T}_\sigma$ begins to form as soon as the rat starts navigating. Every detected instance of place cell coactivity contributes a simplex to $\mathcal{T}_\sigma$. At the early stages of navigation, when only a few cells had time to produce spikes, the coactivity complex is small, fragmented, and contains many holes, most of which do not represent physical obstacles in the environment. Such holes, which may be viewed as transient "gaps" in the cognitive map, tend to disappear as spatial learning continues. The minimal time, T_{min}, after which the topology of $\mathcal{T}_\sigma$ matches the topology of the environment, or more precisely, when the correct number of topological loops emerges, Figure 1C, can therefore be viewed as a theoretical estimate of the time required to learn the hippocampal map [23, 24].

Parameter dependence. An important property of the model is that the structure of the coactivity complex $\mathcal{T}_\sigma$ and the time course of its formation during learning are sensitive to various parameters of the neuronal firing statistics, which allows studying the net effect produced by these parameters on spatial learning. For example, the oscillations of the extracellular electrical field potential, typically referred to as the local field potential (LFP), are known to modulate the place cells' activity at several timescales. First,

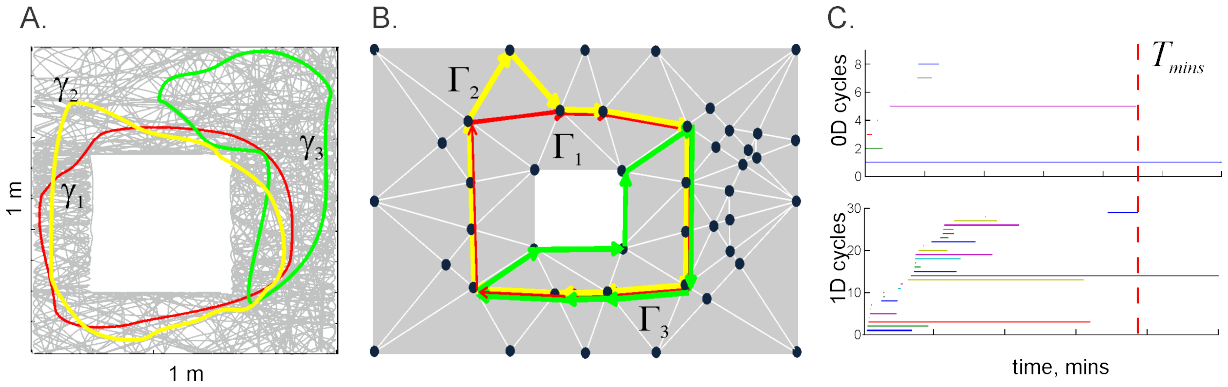

FIG. 1: **Paths in the environment are represented in a simplicial complex**. (**A**) Two topologically equivalent paths in a physical environment, γ_1 and γ_2, encircle an obstacle (white square) that cannot traversed by the rat's trajectory (grey curve in the background) and are therefore non-contractible. The path γ_3 does not encircle the obstacle and therefore is contractible and topologically inequivalent to γ_1 and γ_2. (**B**) A schematic representation of the $2D$ skeleton of the coactivity complex $\mathcal{T}_\sigma$ (vertices shown as black dots, the $1D$ links as white lines and $2D$ facets as grey triangles) and of the simplicial paths Γ_1, Γ_2 and Γ_3, which represent the physical paths γ_1, γ_2 and γ_3. The topological equivalences and inequivalences between the simplicial paths ($\Gamma_1 \cong \Gamma_2$ and $\Gamma_1 \ncong \Gamma_3$, $\Gamma_2 \ncong \Gamma_3$) provide qualitative information about the physical paths, encoded via place cell coactivity. Since we are primarily concerned with representing topological properties of the navigational paths, in the following we discuss only the $2D$ skeleton of the coactivity complex. (**C**) Timelines of the topological loops encoded in the coactivity complex. As the animal begins to explore its environment, the coactivity complex contains many spurious topological loops most of which do not represent the physical obstacle. This "topological noise" disappears after about five minutes, which marks the learning time, T_{min}—the moment when the correct topology of space (one $1D$ loop representing the obstacle and one $0D$ loop that informs us that the environment is connected) has emerged.

each place cell tends to spike within a small range of the phases of the "theta" component of the LFP (θ, 4-12 Hz [32]), which depends on the distance that the animal has traveled into the corresponding place field. As a rat moves through the place field, the preferred θ-range of a place cell progressively decreases with each new θ-cycle, a phenomenon known as the θ-phase precession [33]. The preferred θ-phases of different cells are additionally synchronized by the second major component of the LFP, the "gamma" rhythm (γ, 30-80 Hz, [34]). In fact, the period of the more rapid γ-rhythm, T_γ, is believed to define the range of the preferred phases within the slower θ-rhythm; on average a θ-period, T_θ, contains about seven γ-cycles, $T_\theta \approx 7T_\gamma$ (see [35] and Figure S1A).

Numerous experimental [36–40] and theoretical [35, 41–44] studies demonstrate that both the θ- and the γ-waves play key roles in spatial, working, and episodic memory functions. However, most theoretical analyses addressed the way in which the γ-synchronization affects the informational contents of spiking in small networks or in the individual cells. In contrast, the topological approach allows modeling cognitive map as a whole. For example, it was used in [24] to demonstrate that θ-precession makes otherwise poorly performing ensembles more capable of spatial learning.

The present analysis applies the topological model to study the effect produced on spatial learning by the γ-waves and to demonstrate that γ-synchronization of the place cell spiking activity enables the encoding or retrieval of the large-scale spatial representations of the environment by integrating place cell coactivity at a synaptic timescale.

II. THE MODEL

Computational modeling of the θ-phase precession is relatively straightforward: at the basic level, it amounts to imposing a particular relationship between a place cell's spiking probability, the phase of the

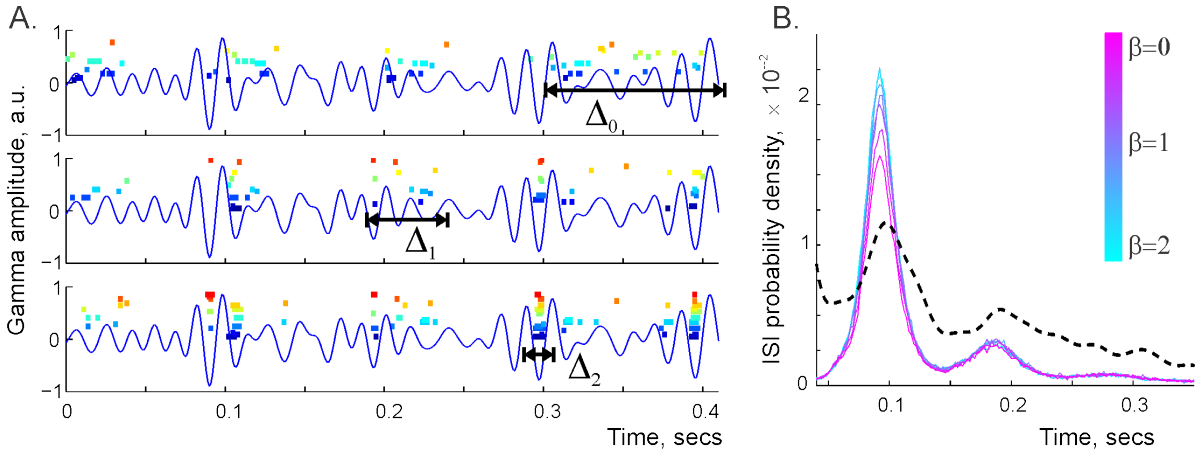

FIG. 2: **Gamma synchronization**. (**A**) Without coupling with the γ-wave ($\beta = 0$, top panel) the simulated place cell spikes are diffusely scattered over the time axis. The temporal spread of the place cell coactivity is about a couple of θ-periods, $\Delta_0 \approx 1.5T_\theta$, $T_\theta \approx 125$ msec. At $\beta = 1$, the intervals of place cell coactivity concentrate near domains of high γ-amplitude, $\Delta_1 \approx 0.5T_\theta$. At $\beta = 2$, the spikes accumulate near the γ-troughs, $\Delta_2 \approx T_\gamma$, thus producing dynamical cell assemblies (bottom panel). (**B**) The statistics of interspike intervals (ISI) for different βs. The black dashed line shows the distribution of the time intervals between deep γ-troughs (deeper than two standard deviations of $A(t)$ from the mean). As β increases, the intervals between spikes are more controlled by the deep troughs (where the amplitude exceeds three standard deviations of $A(t)$ above the mean). Note, that the tendency of spikes produced by the same place cell to appear within the same γ-cycle can be viewed as a basic model of bursting [49].

θ-wave and the distance that the animal has traveled into a corresponding place field [45] (see Methods). However, the effects of the γ-rhythm are more diverse. Electrophysiological experiments suggest that there exist at least two types of place cells: the "TroPyr" cells that spike at the trough of the fast γ-wave (50-80 Hz) and the "RisPyr" cells that fire at the raising phase of slow γ-waves, overriding θ-precession [46–48]. Although our approach allows modeling both cell types (see Methods), in the following we will model only the TroPyr cells that exhibit more robust firing patterns and higher firing rates, and therefore may play a primary role in producing the cognitive map [23, 24].

γ-modulation of spiking. Physiologically, the γ-wave represents fast oscillations of the inhibitory post-synaptic potentials. As the amplitude of γ drops at a certain location, the surrounding cells with high membrane potential spike [50–52]. As a result, the preferred θ-phase of several cells becomes synchronized with a γ-trough, which thereby gates the place cell coactivity. The literature refers to such groups of coactive place cells as "dynamic cell assemblies" (see [57–59]and Figure S1A).

Modeling γ-modulation therefore requires adjusting the times of the θ-modulated spikes closer to the troughs of the γ-wave [54]. Algorithmically, this task is similar to the task of distributing stochastic particles over the wells of a $1D$ potential energy field, which is solved based on the Maximum Entropy Principle [55]. The probability that a particle lands at point x in a potential $U(x)$ is $p \sim e^{-\beta U(x)}$, where the parameter β controls the spread of the locations around the minima of $U(x)$. In statistical physics, this parameter is interpreted as the inverse temperature. Higher values of β, meaning lower temperatures, imply that the particles are more confined to the bottoms of the wells (Figure S1B).

Viewing the γ-amplitude, $A_\gamma(t)$, as an inhibitory potential extended over the time axis, we confined the place cells' firing to the troughs of the γ-wave by modulating their firing rates with the factor $e^{-\beta_\gamma A_\gamma(t)}$. Thus, the parameter β_γ controls the temporal spread Δ_β of spikes produced by the dynamical cell assemblies. For small β_γ, the cell assemblies are "hot," meaning their spikes are spread diffusely near the γ-troughs. For large β_γ the assemblies are "cold," their spikes "freeze" at the γ-troughs (Figure 2 and Figure S2). In particular, the case in which the spike trains are uncorrelated with the γ-troughs corresponds to the limiting case of an "infinitely hot" ($\beta_\gamma = 0$) hippocampus, modeled in [24].

To our knowledge, the statistics of the temporal spreads of the spikes produced by the dynamical cell

assemblies have not been studied. However, neurophysiological literature suggests that a typical spread is about one γ-period ($\Delta \approx T_\gamma \approx 20$ msec) [56–59], which implies that the effective temperature of the hippocampal cell assemblies is comparable to the mean γ-trough amplitude $1/\beta_\gamma \approx \bar{A}_{tr}$ (see Methods). In the following discussion, it will be convenient to scale the amplitude of the γ-wave with its standard deviation from the mean, σ_γ, $A_\gamma(t) \to A(t) = A_\gamma(t)/\sigma_\gamma$. In turn, this entails the corresponding scaling of the inverse temperature, yielding a parameter $\beta = \beta_\gamma \sigma_\gamma$ with the "physiological" range between $0.5 \lesssim \beta \lesssim 2$.

Reading out place cell coactivities. The spiking signals produced by the place cells are transmitted to a population of readout neurons downstream from the hippocampus. In the reader-centric approach to information processing in the hippocampal network [29, 58], these neurons play a defining role. An assembly σ is viewed not simply as an arbitrary combination of coactive place cells but as a functionally interconnected cell group that jointly triggers a spiking response from a certain readout neuron n_σ. In turn, the readout neuron n_σ spikes upon receiving a sufficient amount of timed EPSP inputs over a certain period w_σ, the "integration window" [60–62]. This is the only parameter that describes the readout neurons in the following discussion. Clearly, different readout neurons may integrate inputs over different time intervals. However, in order to simplify the present approach, we will describe the entire population of the readout neurons using a single parameter $w_\sigma = w$, viewed as the average time over which a typical readout neuron accumulates EPSP inputs [24].

θ and γ synchronicity. In our previous study [24], we modeled assemblies of independently θ-precessing place cells simply as combinations of neurons that happened to produce spikes within a certain w-period. The model predicted that the spatial maps are built reliably if the coactivity inputs are identified over the θ-timescale ($T_\theta \lesssim w \lesssim 2T_\theta$). However, as w shrinks, the chance of producing and detecting the coactivities within a w-period diminishes, and the topological map takes longer to form. For the intermediate range of values ($3T_\gamma \lesssim w \lesssim 3T_\theta$), the learning time is approximately inversely proportional to w, but as w reduces to the γ-period, the pool of detected place cell coactivities often fails to capture the topological structure of the environment or requires a much longer time to produce it, exhibiting high variability of T_{min} upon w. Moreover, experimental studies have shown that the synchronicity of the place cell assemblies is best manifested precisely at the γ-timescale [57–59]. This implies that the hippocampal network is capable of producing large-scale spatial maps based on the γ-timescale readouts. Therefore, we hypothesized that the failure of the previous (θ-driven) topological model to do that may be due to poorer synchronization in the assemblies of independent neurons driven by common θ-pacemaker, rather than to the physiological cell assemblies that are additionally synchronized through synaptic interactions [63].

In the present analysis, we use the effective temperature $1/\beta$ to describe phenomenologically these additional synchronization mechanisms. As illustrated in Figure 2, the parameter β controls the temporal spread of the spiking activity in cell assemblies, Δ_β, independently from w and allows transitioning from desynchronized cell assemblies to the cell assemblies that are tightly coupled with γ-troughs. The results shown in Figure 2 also suggest that binding the coactivity of place cell assemblies within γ-periods ($\Delta_2 \approx T_\gamma$) should significantly reduce the time required by the downstream networks to detect place cell coactivity. Thus, γ-synchronization may enable us to construct a reliable neuronal representation of space using the γ-timescale readout, $w \approx T_\gamma$, which would provide a direct demonstration of the importance of the γ-synchronization at the systemic level.

III. RESULTS

To describe the effects of the γ-waves on the ability of place cells to encode spatial information, we built the coactivity complex using γ-modulated spike trains for different βs and studied its topological properties for a set of ws, including the values for which the independently θ-precessing place cells fail to produce correct topological maps. The results shown on Figure 3 demonstrate that, at large integration windows ($w \geq T_\theta$, fat lines), tightening the cell assemblies around the γ-troughs does not produce a significant effect

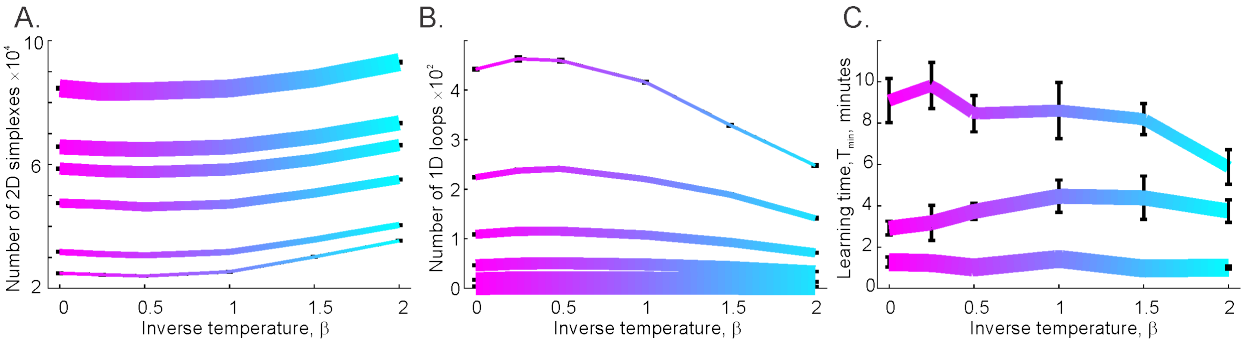

FIG. 3: **Influence of γ-modulation on spatial learning in a cell assembly network with coincidence detector readout neurons.**. There are two major parameters of the model: the mean width of the temporal window w over which the postsynaptic readout neurons integrate spiking inputs from the place cell assemblies ($w_1 = 2T_\theta$, $w_2 = 1.2T_\theta$, $w_3 = 0.8T_\theta$, $w_4 = 0.5T_\theta$, $w_5 = 0.3T_\theta$, $w_6 = 0.2T_\theta$, represented by the thickness of the line), and the effective temperature $1/\beta$ which controls the clustering of place cells' spikes around the troughs of the γ-wave (Figure 2). Larger values of β (indicated by the blue color of the colormap) correspond to tighter coupling between the place cell's spiking probability and the γ-amplitude (Figure S1). (**A**) The number of $2D$ simplexes, N_2, in the coactivity complex $\mathcal{T}_\sigma$ as a function of β, for different ws. For large integration windows (thicker lines), coupling with γ-wave does not produce significant effect: the N_2 changes less along the β-axis. As w decreases, the number of simplexes drops (the thinner lines lay below the thicker ones). However, the smaller is w, the more increase of the number of coactive place cell combination is produced by the cooling of the cell assemblies: for $w = T_\gamma$ (top curve) the number of $2D$ simplexes grows by 40% as β goes from 0 to 2. (**B**) Shrinking the integration window w increases the total number of topological loops observed in $\mathcal{T}_\sigma$ during the course of learning, whereas cooling down the coactivity complex reduces this number. For example, the number of cold loops ($\beta = 2$) at $w = T_\gamma$ is about 50% of the number hot loops ($\beta = 0$). (**C**) The learning time T_{min} grows as w shrinks and tends to decrease as a function of β. Note however, even cold simplicial complexes fail to produce the correct topological maps for small ws. In the particular map illustrated here (mean place field size $s = 24$ cm, mean firing rate $f = 20$ Hz, $N_c = 450$ cells), learning time diverges at $w \geq 0.5T_\theta$.

on either the structure of $\mathcal{T}_\sigma$ or on the times required to learn the map T_min. This outcome is easy to explain: if the readout neurons accumulate EPSPs at the θ-timescale, i.e., over hundreds of milliseconds, the temporal arrangement of the spikes at the γ-timescale does not change the combinations of coactive place cell detected downstream. In other words, no matter how the γ-tuned spikes are spread inside a θ-wide window w, the coactivity simplexes, and hence the coactivity complex, remain the same, yielding the same topological information after the same learning period. As w decreases, the temporal spread of the poorly synchronized, "hot" place cell assemblies begins to exceed w. As a result, only a fraction of the coactive cells can be detected downstream, which leads to a decrease of the number of simplexes in $\mathcal{T}_\sigma$ and to a proliferation of spurious topological loops during the learning period. Moreover, many of these loops persist indefinitely, preventing the appearance of the correct topological information even at the intermediate values of w (Figure 3C).

In contrast, the behavior of the "cold" cell assemblies ($\beta > 1$, the blue ends of the graphs) is different. First, the number of $2D$ simplexes raises with cooling, which reflects the fact that the size of the cell assemblies increases with increasing β (Figure 3A). Second, colder coactivity complexes $\mathcal{T}_\sigma$ yield fewer, faster contracting spurious loops (Figure 3B and Figure S3). Third, the learning times drop significantly: for $\beta = 2$, the T_{min} computed for $w = 0.5T_\theta$ reduce by about 50% compared to the desynchronized, $\beta = 0$ case, which indicates that γ-synchronization allows building a topological map based on the coactivity information transmitted to the downstream networks at times shorter than one γ-cycle (Figure 3C and Figure S4).

Nevertheless, the results shown on Figure 3 typically do not extend to the γ-timescale of w. The inputs collected from the cell assemblies which cooled to the physiological range of βs ($0.5 \lesssim \beta \lesssim 2$) at $w < 0.3T_\theta$ often failed to produce an accurate map of the environment. This suggests that producing a correct neuronal

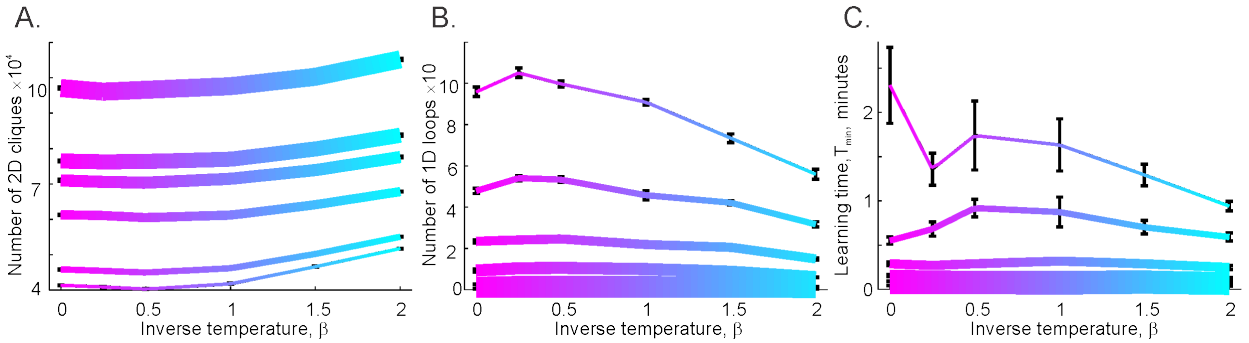

FIG. 4: **Influence of the γ-modulation on spatial learning in cell assembly network with input integrator readout neurons: clique complexes**. (**A**) The dependence of the number of triple connections in the clique coactivity complex $\mathcal{T}_\varsigma$ is similar to the dependence of number of $2D$ simplexes in the simplicial coactivity complex. As the integration window decreases (same range of ws as on Figure 3), the number of triple connections drops. Cooling down the assemblies does not produce significant effect at large integration windows, but increases the number of triple connections for small ws (by about 25% for $w \approx T_\gamma$). (**B**) The total number of topological loops observed in the clique coactivity complex $\mathcal{T}_\varsigma$ is reduced with cooling for small ws, similarly to the case of the Čech coactivity complex. At the γ-timescale, $w \approx T_\gamma$, the tendency of the shrinking ws to produce large numbers of topological loops in the clique coactivity complex is nearly compensated by cooling down $\mathcal{T}_\varsigma$: the number of cold loops ($\beta = 2$) in $\mathcal{T}_\varsigma$ is about 50% of the number hot loops ($\beta = 0$). Note that despite similar qualitative behaviors, the scales of $N^\sigma_{l_1}$, and $N^\varsigma_{l_1}$ are different: the clique complex produces fewer spurious loops than the simplicial complex. (**C**) The learning times grow as a function of w; however, for the clique complex they remain finite even for $w \approx T_\gamma$. Thus, the cooler the ensemble of cell assemblies, the faster it learns, especially for small w.

map of space within a biologically plausible learning time using $w \approx T_\gamma$ requires further cooling of $\mathcal{T}_\sigma$ (by increasing β indefinitely, the cell assemblies can be made as tight as desired). Thus, in order to keep the parameter β within the physiological range, we have deployed an alternative approach.

Clique coactivity complexes. In the above discussion, the central construction of the model, which is the Čech coactivity complex $\mathcal{T}_\sigma$, was introduced as a schematic representation of the place field map [29]. However, as shown in [64, 65], a coactivity complex can be built not only by detecting higher order coactivity events that directly mark the locations were several place field overlap, but also by integrating the information provided by the lower order place cell coactivities. Physiologically, the latter option corresponds to the cell assembly network in which the readout neurons integrate lower order coactivity inputs over a working memory timescale, rather than merely react to coactivities as all-or-none coactivity detectors [66, 67].

To model a network of cell assemblies driving a population of input-integrator readout neurons, we used the following approach. First, we detected the lowest order, pairwise place cell coactivities and used them to build a connectivity graph G (see [64] and Figure S5). Then the maximal cliques of G (see Methods) were identified with the maximal simplexes of a new "clique" coactivity complex $\mathcal{T}_\varsigma$. A key property of this algorithm is that the connections constituting a clique or a simplex do not have to be detected at once—instead, they can be accumulated over an extended period. For physiological accuracy, we restrict this period to 10 mins or less, which results in a coactivity complex whose simplexes, or a cell assembly network whose cell assemblies, emerge over working memory intervals.

Although the algorithm of constructing temporal Čech and the clique complexes seem quite different, the actual difference between these two coactivity complexes is not as significant. First, as shown in [29, 64], most simplexes of $\mathcal{T}_\varsigma$ correspond to the simplexes of $\mathcal{T}_\sigma$ and vice versa (i.e., the identities of the cell assemblies are largely the same, only the time course of their construction changes) and the topological structures of these complexes are quite close. Second, most pairwise connections within the cliques of G are produced almost simultaneously while the rat traverses the region where several place fields overlap. In other words, most cliques appear at once, just as the simplexes do, and only a relatively small number of the

maximal cliques are actually "corrected" over time [65]. Nevertheless, this effect does improve the overall performance of the clique coactivity complexes, which typically produce much smaller numbers of spurious topological loops. This corresponds to a shorter learning times T_{min} than the Čech coactivity complexes.

Implementing the γ-synchronization mechanism in an integrator model yields the results illustrated in Figure 4. First, the structure of the graphs on Figures 3A and Figure 4A is qualitatively similar, though the pool of the third order cliques comes out to be slightly larger than the pool of $2D$ simplexes. This is because not every clique makes a simultaneous appearance as a simplex, but every simplex can be viewed as an instantly detected clique. The behaviors of the topological loops in $\mathcal{T}_\varsigma$ and in $\mathcal{T}_\sigma$, shown in Figures 3B and Figure 4B are similar as well: the γ-synchronization reduces the number of the cold spurious loops in both types of complexes (Figure S6). Physiologically, this implies that γ-rhythm produces the same organizing effect on the activity of cell assembly network, whether the latter is based coincidence detector or on the input integrator readout neurons. However, it should be noted that, for all βs, the number of loops in $\mathcal{T}_\varsigma$ is smaller than in $\mathcal{T}_\sigma$ by an order of magnitude, which illustrates the efficiency of the input integrating readout neurons. Most importantly, the integrator complex $\mathcal{T}_\varsigma$ produces finite learning times at the γ-timescale integration window, $w \approx T_\gamma$, which demonstrates that the hippocampal network can produce a spatial memory map by reading out γ-synchronized place cell coactivity at the γ-timescale and accumulating them over working memory timescale, and the model provides a simple phenomenological mechanism for this demonstration.

IV. DISCUSSION

The neuronal activity is synchronized across the hippocampal network, giving rise to rhythmic flows of synaptic currents. The resulting waves of the mean extracellular field define the timescales of the place cell (co)activity and hence control the "parcellation" of the information flow which is received by downstream networks. In particular, the synchronization of the processes taking place at the synaptic timescale, such as the processes controlled by the membrane time constant, by the duration of receptor-mediated postsynaptic spike potentials, by the rate of spike-timing dependent plasticity and so forth ([68–70]) is manifested at the network level as γ-frequency oscillations [71–75]. Processes that involve slower forms of synaptic plasticity, including slow changing spiking thresholds [76–79], synchronize at the timescales of θ-frequencies. As a result, θ-oscillations provide lower resolution temporal packaging of place cell coactivity [63, 80, 81], which allows integrating spiking inputs from several cell assemblies over one or more θ-periods [82–84].

The topological model based on independently θ-precessing place cells provides a self-consistent description of the hippocampal network's function at the θ-timescale, predicting, in particular, an optimal integration window for reading out the information within the θ-range [24]. However, as the integration window becomes smaller, the spatial map encoded by independently precessing place cells fails to represent spatial maps, indicating the importance of additional synchronization at the γ-timescale and suggesting that further refinement of the model is required.

The phenomenological model proposed above is based on the assumption that the γ-rhythm controls not only the probability of the cell assemblies' spiking but also defines the temporal spread of the spikes produced by the cell assemblies around the troughs of the γ-wave. As a result, the model predicts that if the preferred θ-phases synchronize with the γ-troughs, the topological map of space can be robustly captured by integrating the place cell coactivity at the γ-timescale. Thus, γ-synchronization of spiking activity is crucial for encoding and reading out the large scale information by acquiring the information from the cell assembly inputs arriving in "γ-packets" [58].

Second, the model can explain why a suppression of the γ-wave amplitude, induced by the changes in network's synaptic physiology [85–89], or produced by psychoactive drugs [90] such as cocaine [91, 92], or arising due to neurodegeneration or aging [93, 94], usually correlates with impairments in learning. Lastly, these results may also explain the well-known correlation between successful learning and retrieval of the

learned information with the increase of the γ-amplitude in raised attention states [95–99].

V. ACKNOWLEDGMENTS

We thank Robert Phenix for editing the manuscript. The work was supported in part by the NSF 1422438 grant (E.B. and Y.D.) Houston Bioinformatics Endowment Fund the W. M. Keck Foundation grant for pioneering research (M.A. and Y.D.)

VI. METHODS

Glossary. An *abstract simplex* of order d, σ^d, is a set of $(d+1)$ elements, e.g., a set of $(d+1)$ active cells. Note that the subsets of the set σ^d form subsimplexes of σ^d and that a nonempty overlap of any two simplexes σ_1^d and σ_2^d is a subsimplex of both σ_1^d and σ_2^d. A *simplicial complex* Σ_σ is a family of simplexes. The elements of a simplex σ^d can be visualized as vertices of d-dimensional polytopes: σ^0 can be visualized as a point, σ^1 as the ends of a line segment, σ^2 as the vertices of a triangle, σ^3 as the vertices of a tetrahedron, etc. [100]. A *clique* in a graph G is a set of fully interconnected vertices (i.e., a complete graph). Combinatorically, cliques have the same key properties as the abstract simplexes: any subcollection of vertices in a clique is fully interconnected, and hence forms a subclique. A nonempty overlap of two cliques ς_1^d and ς_2^d is a subclique in both ς_1^d and ς_2^d. Thus, cliques define abstract simplexes and hence the collection of cliques in a graph G defines a *clique simplicial complex* $\Sigma_\varsigma(G)$.

Choice of the simulated environment. In [24] we showed that the time required to learn a large spatial environment is approximately equal to sum of times required to learn its parts. We therefore simulated a non-preferential exploratory behavior in a small planar environment ($1m \times 1m$) shown in Figure 1A, which is similar to the ones used in electrophysiological experiments [101].

The **Poisson spiking rate** of a place cell c at a point $r(t) = (x(t), y(t))$ is given by

$$\lambda_c(r) = f_c e^{-\frac{(r-r_c)^2}{2s_c^2}}$$

where f_c is the maximal firing rate and s_c defines the size of the place field centered at $r_c = (x_c, y_c)$. The set of s_cs and f_cs in an ensemble of N place cells are lognormally distributed around a certain ensemble-mean firing rate, f and a certain ensemble-mean place field size s, with the variances $\sigma_f = af$ and $\sigma_s = bs$ respectively, i.e., a place cell ensemble is described by a triple of parameters: (s, f, N) [23].

θ-phase precession. As the rat moves over a distance $l(t)$ into the place field of a cell c, the preferred spiking phase is

$$\varphi_{\theta,c}(t) \approx 2\pi(1 - l(t)/L_c),$$

where $L_c \sim 3s_c$ is the size of the place field [33, 102]. To simulate the coupling between the firing rate and the θ-phase, we modulated the original Gaussian firing rate by a θ-factor $\Lambda_{\theta,c}(\varphi)$, giving

$$\Lambda_{\theta,c}(\varphi) = e^{-\frac{(\varphi-\varphi_{\theta,c}(t))^2}{2\varepsilon_c^2}},$$

using the θ-component of the LFP recorded in wild type mice. The width, ε, of the Gaussian was defined in [24] to be the ratio of the mean distance that rat travels during one θ-cycle to the size of the place field, $\varepsilon = 2\pi v/L\omega_\theta$, where v is the rat's speed and $\omega_\theta/2\pi$ is the frequency of the θ-signal.

γ-modulation. To incorporate the γ-rhythm into our model, we extracted the 30-80 Hz frequency band from the same LFP signal so that all the existing correlations between θ and γ waves are preserved, and

shifted the simulated place cells' spiking times towards the troughs of γ amplitude by modulating their respective spiking rates with the additional Boltzmann factor [55],

$$\Lambda_\gamma(t) \sim e^{-\beta_\gamma A_\gamma(t)}, \tag{1}$$

where $A_\gamma(t)$ is the amplitude of the γ-wave and $1/\beta_\gamma$ is a formal parameter that plays the role of the effective temperature [103] (Figure 2). Simulating the net firing rate as a product of all three factors

$$\lambda_{net} = \lambda_c(x, y)\Lambda_{\theta,c}(\varphi)\Lambda_\gamma(A_\gamma)$$

preserves spatial selectivity of spiking and the θ-precession (Figure S7) and forces the preferred phases of the θ-phase precession φ_c into the γ-cycles, in accordance with the θ-γ theory [35, 38, 53].

Temperature of the cell assemblies. In a vicinity of the i^{th} trough, the gamma signal has the form

$$A_\gamma(t) \approx A_{\gamma,0} - A_{\gamma,i}\cos(\omega_i t) \approx a_{\gamma,i} + A_{\gamma,i}\frac{\omega_i^2 t^2}{2}, \tag{2}$$

where the parameters $A_{\gamma,0}$, $A_{\gamma,i}$ and ω_i define the mean level of A_γ, its instantaneous amplitude, and the instantaneous frequency at the i^{th} trough, and $a_{\gamma,i} = A_{\gamma,0} - A_{\gamma,i}$. Using the expansion (2) in (1) allows estimating the spread Δ_i of the spikes around the i^{th} through from the Gaussian variance

$$\Delta_i^2 = \frac{1}{\beta_\gamma A_\gamma \omega_i^2}.$$

This variance is about six times smaller than the instantaneous period, $6\Delta_i \approx T_i = 2\pi/\omega_i$.Hence

$$\frac{6}{\sqrt{\beta_\gamma A_\gamma}\omega_i} \approx \frac{2\pi}{\omega_i}$$

which implies that the effective temperature is approximately equal to the amplitude

$$\frac{1}{\beta_\gamma} \approx A_{\gamma,i}.$$

Although the "effective temperature" β_γ may differ between different cell assemblies and different γ-troughs, we consider the simplified case in which a single parameter β defines the mean coupling between the γ-wave's amplitude and frequency and the place cell's spike times across the entire place cell network. By normalizing the amplitude A_γ by the $\sigma_\gamma = \left\langle \sqrt{A_\gamma^2 - A_0^2} \right\rangle_t$, $A = A_\gamma/\sigma_\gamma$, we get the scaled parameter $\beta = \beta_\gamma\sigma_\gamma$, with the characteristic value

$$\beta = \frac{1}{A}.$$

Cell types. The described approach can be applied to both the TroPyr and the RisPyr cells. Mathematically, the "raising phases of γ" that controls spiking of the RisPyr cells correspond to the vicinities of peaks of the γ-amplitude's time derivative. Hence, the spiking probability of the RisPyr can be constrained by a factor similar to (1), involving the derivative of the γ-amplitude, $A'(t)$, which would overridden the θ-precession constraint ($\Lambda_{\theta,c}(\varphi) = 1$) in the vicinity of the $A'(t)$-peaks. The analysis of the mixed (RisPyr and TroPyr) ensembles is more complex and requires a discussion *sui generis*.

Mathematical methods required for this study are based on the Persistent Homology Theory (see [23] and [104, 105]) implemented in "JPlex" freeware package [106].

VII. REFERENCES

[1] Best PJ, White AM, Minai A (2001) Spatial processing in the brain: the activity of hippocampal place cells, *Ann. Rev. Neurosci.* 24: 459-486.

[2] Jensen O, Lisman JE (2000) Position reconstruction from an ensemble of hippocampal place cells: contribution of theta phase coding, *J. Neurophysiol.* 83: 2602-2609.

[3] Pfeiffer, B. Foster, D. (2013). Hippocampal place-cell sequences depict future paths to remembered goals, *Nature* **497**, 7479.

[4] Carr MF, Jadhav SP, Frank LM (2011) Hippocampal replay in the awake state: a potential substrate for memory consolidation and retrieval, *Nat. Neurosci.*, 14: 147-153.

[5] Ji D, Wilson MA (2007) Coordinated memory replay in the visual cortex and hippocampus during sleep, *Nat. Neurosci.* 10: 100-107.

[6] Kim SM, Frank LM (2009) Hippocampal lesions impair rapid learning of a continuous spatial alternation task, *PLoS One* 4: e5494.

[7] Savage LM, Buzzetti RA, Ramirez DR (2004) The effects of hippocampal lesions on learning, memory, and reward expectancies, *Neurobiol. Learn. Mem.*, 82: 109-119.

[8] McNamara TP, Shelton AL, Shelton AL (2003) Cognitive maps and the hippocampus, *Trends Cogn. Sci.* 7: 333-335.

[9] O'Keefe J, Nadel L (1978) *The hippocampus as a cognitive map*, New York: Clarendon Press; Oxford University Press. xiv, 570 pp.

[10] Alvernhe A, Sargolini F, Poucet B (2012) Rats build and update topological representations through exploration, *Anim. Cogn.* 15: 359-368.

[11] Wu X, Foster DJ. (2014) Hippocampal Replay Captures the Unique Topological Structure of a Novel Environment, *J. Neurosci.* 34: 6459-6469.

[12] Dabaghian Y, Brandt VL, Frank LM (2014) Reconceiving the hippocampal map as a topological template, *eLife* 10.7554/eLife.03476.

[13] Diba K, Buzsaki G (2008) Hippocampal network dynamics constrain the time lag between pyramidal cells across modified environments, *J. Neurosci.* 28: 13448-13456.

[14] Poucet B, Herrmann T (2001) Exploratory patterns of rats on a complex maze provide evidence for topological coding, *Behav. Processes* 53: 155-162.

[15] Gothard KM, Skaggs WE, McNaughton BL (1996) Dynamics of mismatch correction in the hippocampal ensemble code for space: interaction between path integration and environmental cues, *J. Neurosci.* 16: 8027-8040.

[16] Leutgeb JK, Leutgeb S, Treves A, Meyer R, Barnes CA, et al. (2005) Progressive transformation of hippocampal neuronal representations in "morphed" environments, *Neuron* 48: 345-358.

[17] Wills TJ, Lever C, Cacucci F, Burgess N, O'Keefe J. (2005) Attractor dynamics in the hippocampal representation of the local environment, *Science* 308: 873-876.

[18] Touretzky DS, Weisman WE, Fuhs MC, Skaggs WE, Fenton AA, et al. (2005) Deforming the hippocampal map, *Hippocampus* 15: 41-55.

[19] Cheng J, Ji D (2013) Rigid firing sequences undermine spatial memory codes in a neurodegenerative mouse model *eLife* 2013;2:e00647

[20] Chen Z, Gomperts SN, Yamamoto J, Wilson MA (2014) Neural representation of spatial topology in the rodent hippocampus, *Neural Comput.* 26: 1-39.

[21] Chen Z, Kloosterman F, Brown E, Wilson M (2012) Uncovering spatial topology represented by rat hippocampal population neuronal codes. *J. Comput. Neurosci.*, 33: 227-255.

[22] Curto C, Itskov V (2008) Cell groups reveal structure of stimulus space, *PLoS Comput. Biol.* 4: e1000205.

[23] Dabaghian Y, Mmoli F, Frank L, Carlsson G (2012) A Topological Paradigm for Hippocampal Spatial Map Formation Using Persistent Homology, *PLoS Comput. Biol.* 8: e1002581.

[24] Arai M, Brandt V, Dabaghian Y (2014) The Effects of Theta Precession on Spatial Learning and Simplicial Complex Dynamics in a Topological Model of the Hippocampal Spatial Map, *PLoS Comput. Biol.* 10: e1003651.

[25] Muller RU, Stead M, Pach J. (1996) The hippocampus as a cognitive graph, *J. Gen. Physiol.* 107: 663-694.

[26] Burgess N, O'Keefe J. (1996) Cognitive graphs, resistive grids, and the hippocampal representation of space, *J. Gen. Physiol.* 107: 659-662.

[27] Cheng S (2013) The CRISP theory of hippocampal function in episodic memory, *Front. Neural Circuits* 7.

[28] Samsonovich A, McNaughton BL (1997) Path integration and cognitive mapping in a continuous attractor neural network model, *J. Neurosci.* 17: 5900-5920.

[29] Babichev A, Cheng S, Dabaghian YA (2016) Topological schemas of cognitive maps and spatial learning, *Front. Comput. Neurosci.* 10.

[30] Novikov SP (2004) Discrete connections and linear difference equations, *Tr. Mat. Inst. Steklova* 247: 186–201.

[31] Dabaghian Y (2016) Geometry of Spatial Memory Replay, Neuronal Computation, (arXiv:1508.06579)

[32] Buzski G, Anastassiou CA, Koch C (2012) The origin of extracellular fields and currents—EEG, ECoG, LFP and spikes, *Nat. Rev. Neurosci.* 13: 407-420.

[33] Huxter JR, Senior TJ, Allen K, Csicsvari J. (2008) Theta phase-specific codes for two-dimensional position, trajectory and heading in the hippocampus, *Nat. Neurosci.* 11: 587-594.

[34] Colgin LL, Moser EI (2010) Gamma oscillations in the hippocampus, *Physiology* (Bethesda) 25: 319-329.

[35] Lisman J, Idiart M (1995) Storage of 7 +/- 2 short-term memories in oscillatory subcycles, *Science* 267: 1512-1515.

[36] Shirvalkar PR, Rapp PR, Shapiro ML (2010) Bidirectional changes to hippocampal theta-gamma comodulation predict memory for recent spatial episodes, *Proc. Natl. Acad. Sci. USA*, 107 (15) pp. 70547059.

[37] Tort AB, Komorowski RW, Manns JR, Kopell NJ, Eichenbaum H (2009) Theta-gamma coupling increases during the learning of item-context associations, *Proc. Natl. Acad. Sci. USA* 106: 20942-20947.

[38] J. (2010) Working memory: the importance of theta and gamma oscillations, *Curr. Biol.* 20: R490-492.

[39] Nyhus E, Curran T (2010) Functional role of gamma and theta oscillations in episodic memory, *Neurosci. Biobehav Rev.* 34: 1023-1035.

[40] Duzel E, Penny WD, Burgess N (2010) Brain oscillations and memory, *Curr. Opin. Neurobiol.* 20: 143-149.

[41] Koene RA, Hasselmo ME (2007) First-in-first-out item replacement in a model of short-term memory based on persistent spiking,*Cereb. Cortex* 17: 1766-1781.

[42] Jensen O, Lisman JE (1998) An oscillatory short-term memory buffer model can account for data on the Sternberg task, *J. Neurosci.* 18: 10688-10699.

[43] Zhang X, Kendrick KM, Zhou H, Zhan Y, Feng J. (2012) A Computational Study on Altered Theta-Gamma Coupling during Learning and Phase Coding, *PLoS One* 7: e36472.

[44] Hasselmo ME (2012) How we remember : brain mechanisms of episodic memory. Cambridge, Mass. :: MIT Press.

[45] Lengyel M, Huhn Z, Érdi P (2005) Computational theories on the function of theta oscillations, *Biol. Cybern.* 92: 393-408.

[46] Senior TJ, Huxter JR, Allen K, O'Neill J, Csicsvari J. (2008) Gamma oscillatory firing reveals distinct populations of pyramidal cells in the CA1 region of the hippocampus, *J. Neurosci.* 28: 2274-2286.

[47] Osipova D, Takashima A, Oostenveld R, Fernandez G, Maris E, et al. (2006) Theta and gamma oscillations predict encoding and retrieval of declarative memory, *J. Neurosci.* 26: 7523-7531.

[48] Yamamoto J, Suh J, Takeuchi D, Tonegawa S (2014) Successful Execution of Working Memory Linked to Synchronized High-Frequency Gamma Oscillations, *Cell* 157: 845-857.

[49] Smith AC, Gerrard JL, Barnes CA, McNaughton BL (2000) Effect of age on burst firing characteristics of rat hippocampal pyramidal cells, *Neuroreport* 11: 3865-3871.

[50] Jia X, Kohn A (2011) Gamma rhythms in the brain, *PLoS Biol.* 9: e1001045.

[51] Nikoli D, Fries P, Singer W (2013) Gamma oscillations: precise temporal coordination without a metronome, *Trends Cogn. Sci.* 17: 54-55.

[52] Buzsaki G, Wang XJ. (2012) Mechanisms of gamma oscillations, *Ann. Rev. Neurosci.* 35: 203-225.

[53] Lisman J. (2005) The theta/gamma discrete phase code occuring during the hippocampal phase precession may be a more general brain coding scheme, *Hippocampus* 15: 913-922.

[54] Colgin LL, Denninger T, Fyhn M, Hafting T, Bonnevie T, et al. (2009) Frequency of gamma oscillations routes flow of information in the hippocampus, *Nature* 462: 353-357.

[55] Guiasu S, Shenitzer A (1985) The principle of maximum entropy. The Mathematical Intelligencer 7: 42-48.

[56] Buzski G, Draguhn A (2004) Neuronal Oscillations in Cortical Networks, *Science* 304: 1926-1929.

[57] Harris KD, Csicsvari J, Hirase H, Dragoi G, Buzsaki G (2003) Organization of cell assemblies in the hippocampus, *Nature* 424: 552-556.

[58] Buzsaki G (2010) Neural syntax: cell assemblies, synapsembles, and readers, *Neuron* 68: 362-385.
[59] Harris KD (2005) Neural signatures of cell assembly organization, *Nat. Rev. Neurosci.* 6: 399-407.
[60] Magee JC (2000) Dendritic integration of excitatory synaptic input, *Nat. Rev. Neurosci.* 1: 181-190.
[61] London M, Husser M (2005) Dendritic Computation, *Ann. Rev. Neurosci.* 28: 503-532.
[62] Spruston N (2008) Pyramidal neurons: dendritic structure and synaptic integration, *Nat. Rev. Neurosci.* 9: 206-221.
[63] Dragoi G, Buzsaki G (2006) Temporal encoding of place sequences by hippocampal cell assemblies, *Neuron* 50: 145-157.
[64] Babichev A, Memoli F, Ji D, Dabaghian Y (2015) Combinatorics of Place Cell Coactivity and Hippocampal Maps (arXiv:1509.01677)
[65] Hoffmann K, Babichev A, Dabaghian Y (2016) Topological mapping of 3D space in bat hippocampi. (arXiv:1601.04253)
[66] Knig P, Engel AK, Singer W (1996) Integrator or coincidence detector? The role of the cortical neuron revisited, *Trends Neurosci.* 19: 130-137.
[67] Ratt S, Lankarany M, Rho Y-A, Patterson A, Prescott SA (2015) Subthreshold membrane currents confer distinct tuning properties that enable neurons to encode the integral or derivative of their input, *Front,* Cell *Neurosci.* 8.
[68] Johnston D, Wu SM-s (1995) Foundations of cellular neurophysiology. Cambridge, Mass.: MIT Press. xxxi, 676 pp.
[69] JC, Johnston D (1997) A Synaptically Controlled, Associative Signal for Hebbian Plasticity in Hippocampal Neurons, *Science* 275: 209-213.
[70] Bi G-q, Poo M-m (2001) Synaptic Modification by Correlated Activity: Hebb's Postulate Revisited, *Ann. Rev. Neurosci.* 24: 139-166.
[71] Traub RD, Spruston N, Soltesz I, Konnerth A, Whittington MA, et al. (1998) Gamma-frequency oscillations: a neuronal population phenomenon, regulated by synaptic and intrinsic cellular processes, and inducing synaptic plasticity, *Prog. Neurobiol.* 55: 563-575.
[72] Atallah BV, Scanziani M (2009) Instantaneous Modulation of Gamma Oscillation Frequency by B alancing Excitation with Inhibition, *Neuron* 62: 566-577.
[73] Bartos M, Vida I, Jonas P (2007) Synaptic mechanisms of synchronized gamma oscillations in inhibitory interneuron networks, *Nat. Rev. Neurosci.* 8: 45-56.
[74] Csicsvari J, Jamieson B, Wise KD, Buzsaki G (2003) Mechanisms of gamma oscillations in the hippocampus of the behaving rat, *Neuron* 37: 311-322.
[75] Whittington MA, Traub RD, Kopell N, Ermentrout B, Buhl EH (2000) Inhibition-based rhythms: experimental and mathematical observations on network dynamics, *Int. J. Psychophysiol.* 38: 315-336.
[76] Huerta PT, Lisman JE (1995) Bidirectional synaptic plasticity induced by a single burst during cholinergic theta oscillation in CA1 in vitro, *Neuron* 15: 1053-1063.
[77] Monyer H, Sprengel R, Schoepfer R, Herb A, Higuchi M, et al. (1992) Heteromeric NMDA Receptors: Molecular and Functional Distinction of Subtypes, *Science* 256: 1217-1221.
[78] Henze DA, Buzsaki G (2001) Action potential threshold of hippocampal pyramidal cells in vivo is increased by recent spiking activity, *Neuroscience* 105: 121-130.
[79] Mickus T, Jung H, Spruston N (1999) Properties of slow, cumulative sodium channel inactivation in rat hippocampal CA1 pyramidal neurons, *Biophys. J.* 76: 846-860.
[80] Hasselmo ME, Bodelon C, Wyble BP (2002) A proposed function for hippocampal theta rhythm: separate phases of encoding and retrieval enhance reversal of prior learning, *Neural Comput.* 14: 793-817.
[81] Hasselmo ME (2005) What is the function of hippocampal theta rhythm?–Linking behavioral data to phasic properties of field potential and unit recording data, *Hippocampus* 15: 936-949.
[82] Ang CW, Carlson GC, Coulter DA (2005) Hippocampal CA1 Circuitry Dynamically Gates Direct Cortical Inputs Preferentially at Theta Frequencies, *J. Neurosci.* 25: 9567-9580.
[83] Maurer AP, Cowen SL, Burke SN, Barnes CA, McNaughton BL (2006) Organization of hippocampal cell assemblies based on theta phase precession, *Hippocampus* 16: 785-794.
[84] Mizuseki K, Sirota A, Pastalkova E, Buzsaki G (2009) Theta oscillations provide temporal windows for local circuit computation in the entorhinal-hippocampal loop, *Neuron* 64: 267-280.
[85] Hormuzdi SG, Pais I, LeBeau FEN, Towers SK, Rozov A, et al. (2001) Impaired Electrical Signaling Disrupts Gamma Frequency Oscillations in Connexin 36-Deficient Mice, *Neuron* 31: 487-495.
[86] Buhl DL, Harris KD, Hormuzdi SG, Monyer H, Buzsaki G (2003) Selective impairment of hippocampal

gamma oscillations in connexin-36 knock-out mouse in vivo, *J. Neurosci.* 23: 1013-1018.
[87] McHugh TJ, Blum KI, Tsien JZ, Tonegawa S, Wilson MA (1996) Impaired Hippocampal Representation of Space in CA1-Specific NMDAR1 Knockout Mice, *Cell* 87: 1339-1349.
[88] Frisch C, Souza-Silva MAD, Shl G, Gldenagel M, Willecke K, et al. (2005) Stimulus complexity dependent memory impairment and changes in motor performance after deletion of the neuronal gap junction protein connexin36 in mice, *Behav. Brain Res.* 157: 177-185.
[89] Cho Kathleen KA, Hoch R, Lee Anthony T, Patel T, Rubenstein John LR, et al. Gamma Rhythms Link Prefrontal Interneuron Dysfunction with Cognitive Inflexibility in Dlx5/6(+/-) Mice, *Neuron* 85: 1332-1343.
[90] Whittington MA, Faulkner HJ, Doheny HC, Traub RD (2000) Neuronal fast oscillations as a target site for psychoactive drugs, *Pharmacology & Therapeutics* 86: 171-190.
[91] McCracken CB, Grace AA (2013) Persistent Cocaine-Induced Reversal Learning Deficits Are Associated with Altered Limbic Cortico-Striatal Local Field Potential Synchronization, *J. Neurosci.* 33: 17469-17482.
[92] Dilgen JE, Tompa T, Saggu S, Naselaris TD, Lavin A (2013) Optogenetically evoked gamma oscillations are disturbed by cocaine administration, *Front,* Cell *Neurosci.* 7.
[93] Vreugdenhil M, Toescu EC (2005) Age-dependent reduction of oscillations in the mouse hippocampus in vitro, *Neuroscience* 132: 1151-1157.
[94] Lu CB, Hamilton JB, Powell AD, Toescu EC, Vreugdenhil M (2011) Effect of ageing on CA3 interneuron sAHP and gamma oscillations is activity-dependent, *Neurobiol. Aging* 32: 956-965.
[95] Howard MW, Rizzuto DS, Caplan JB, Madsen JR, Lisman J, et al. (2003) Gamma oscillations correlate with working memory load in humans, *Cereb. Cortex 13*: 1369-1374.
[96] van Vugt MK, Schulze-Bonhage A, Litt B, Brandt A, Kahana MJ. (2010) Hippocampal Gamma Oscillations Increase with Memory Load, *J. Neurosci.* 30: 2694-2699.
[97] Moretti DV, Fracassi C, Pievani M, Geroldi C, Binetti G, et al. (2009) Increase of theta/gamma ratio is associated with memory impairment, *Clinical Neurophysiology* 120: 295-303.
[98] Lundqvist M, Herman P, Lansner A (2011) Theta and Gamma Power Increases and Alpha/Beta Power Decreases with Memory Load in an Attractor Network Model, *J. Cogn. Neurosci.* 23: 3008-3020.
[99] Trimper JB, Stefanescu RA, Manns JR (2014) Recognition memory and theta-gamma interactions in the hippocampus, *Hippocampus* 24: 341-353.
[100] Aleksandrov PS (1965) *Elementary concepts of topology*, New York: F. Ungar. Pub. Co. 63 pp.
[101] Mamad O, McNamara HM, Reilly RB, Tsanov M (2015) Medial septum regulates the hippocampal spatial representation, *Front. Behav. Neurosci.* 9.
[102] Buzsaki G (2002) Theta oscillations in the hippocampus, *Neuron* 33: 325-340.
[103] Jaynes ET (1957) Information Theory and Statistical Mechanics, *Physical Review* 106: 620-630.
[104] Carlsson G (2009) Topology and data, *Bull. Amer. Math. Soc. (NS)* 46: 255–308.
[105] Zomorodian A, and Carlsson, G. (2005) Computing persistent homology, *Discrete & Computational Geometry* 33: 249–274.
[106] (JPlex freeware) (2011). Computational Topology group, Stanford University.

VIII. SUPPLEMENTARY FIGURES

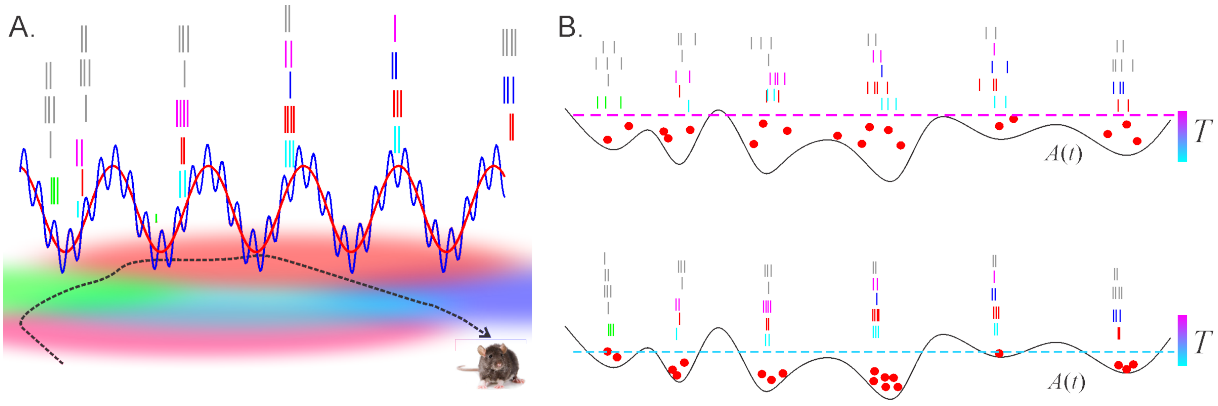

FIG. S1: **Brain rhythms modulate place cell spiking activity**. (**A**). Spike times precess with the θ-rhythm (red wave): as the rat progresses through a place field, the corresponding place cell discharges at a progressively earlier phase in each new θ-cycle. These "preferred" phases of the θ-rhythm correspond to particular γ-cycles; the blue wave shows the net $\theta + \gamma$ amplitude. The synchronized spikes (shown by tickmarks colored according to the place fields traversed by the animal's trajectory) cluster over the γ-troughs, yielding dynamical cell assemblies. (**B**) The spread of spike times around the γ-troughs, by analogy with stochastic particles in a $1D$ potential (black curve). If the temperature is high (dashed line, top panel), the particles (red dots) spread diffusely over the potential landscape, and when the temperature is low (bottom panel), they are confined at the bottoms of the potential wells. A similar effect is produced if the place cells' firing rate is modulating by the Boltzmann factor $e^{-\beta_\gamma A_\gamma(t)}$, where $A_\gamma(t)$ is the amplitude of the γ-wave and β_γ represents the inverse temperature. When β_γ is low, the dynamical cell assemblies are "hot" (i.e., more spread in time), and when β_γ is large, the spikes are concentrated at the γ-troughs.

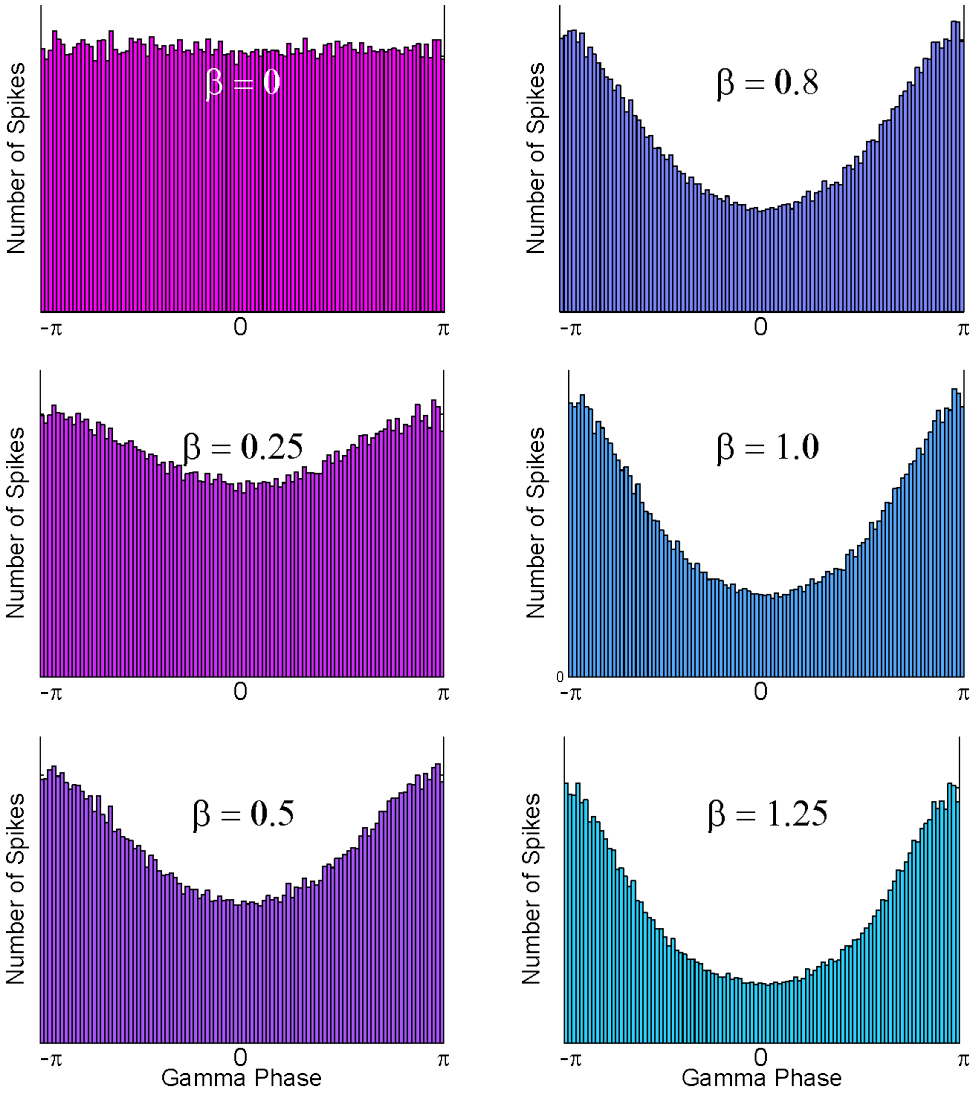

FIG. S2: **Histograms of the γ-phases at the times of place cell spiking**, as a function of the inverse effective temperature β. The cooler the cell assemblies, the more the spikes are coupled with the γ-troughs.

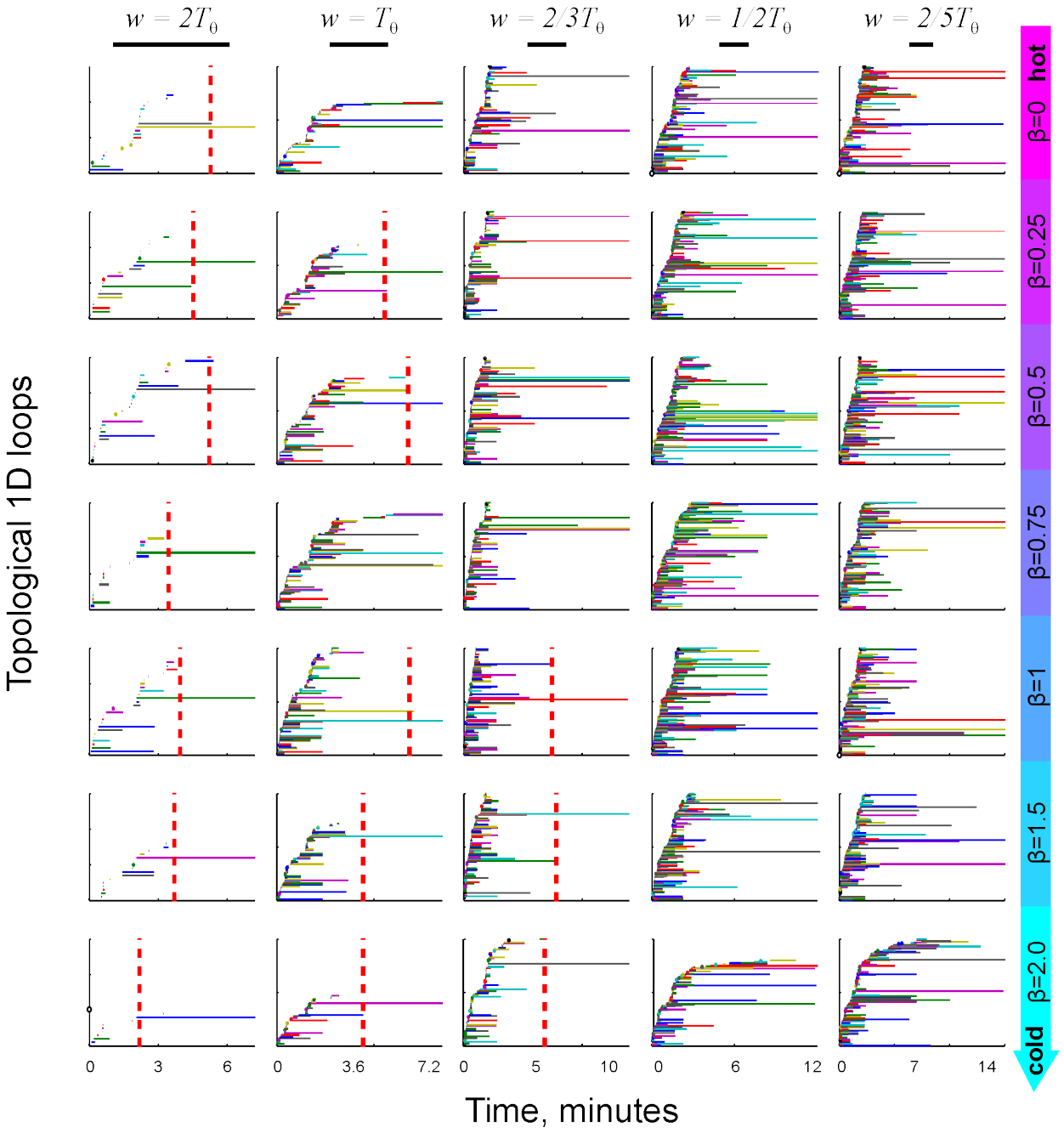

FIG. S3: **Freezing out spurious loops**. Timelines of the topological loops in the coactivity complex produced in the environment shown in Figure 1 for different integration windows (scale of ws is shown on top) and for different effective temperatures $1/\beta$ (colorbar on the right). As the width of the integration window decreases, the number of spurious topological loops in the coactivity complex increases. For large ws, spurious loops tend to disappear with learning (the times T_{min} when the correct topological structure of $\mathcal{T}_\sigma$ emerges are marked by vertical dashed lines). For small ws, some of these loops persist, indicating that the detected coactivity information is insufficient for eliminating spurious holes in $\mathcal{T}_\sigma$. However, cooling down the coactivity complex suppresses the proliferation of the spurious loops: at $\beta = 2$ (bottom row) the coactivity complex has a correct structure at the integration window $w \approx (2/3)T_\theta$.

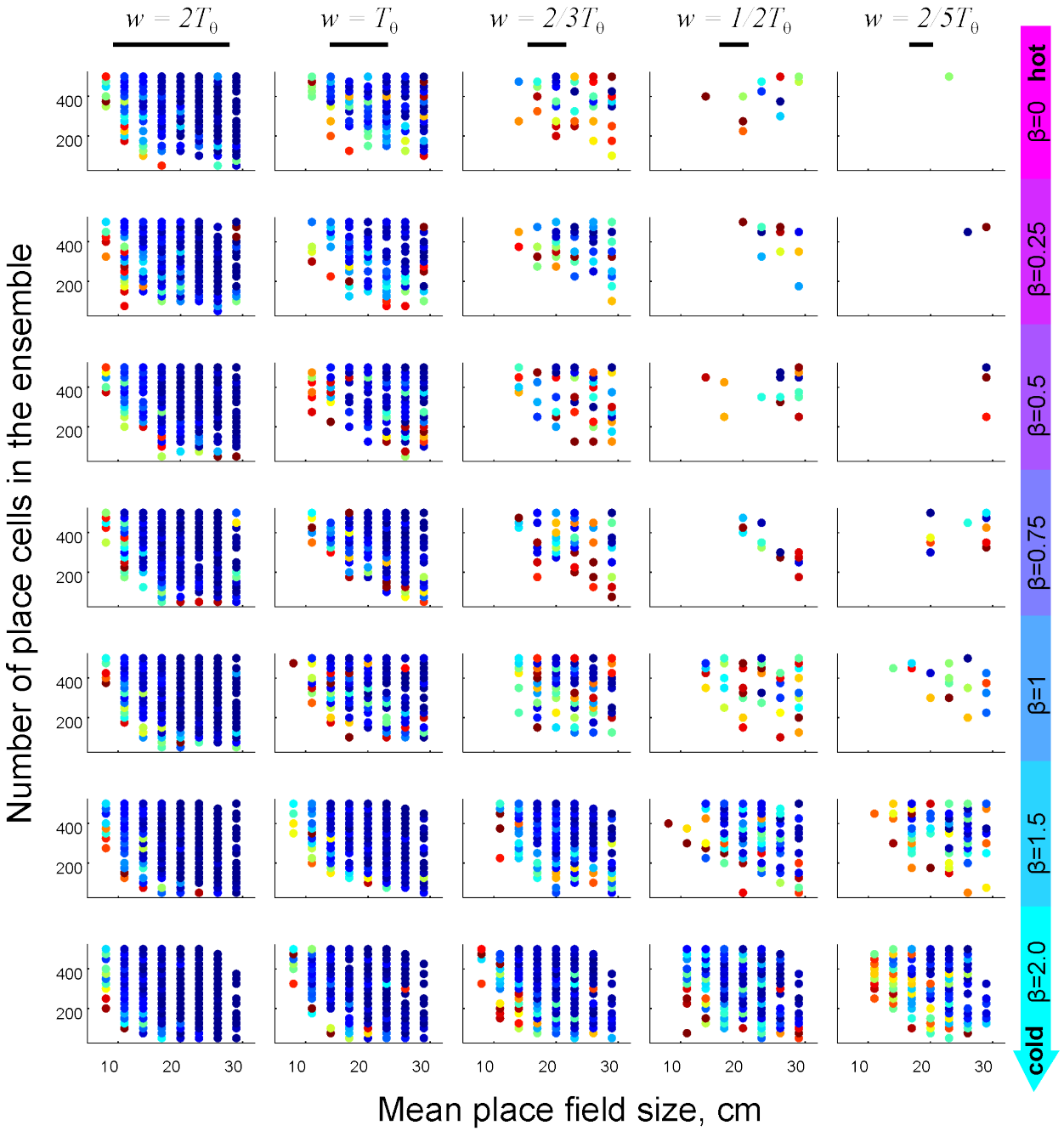

FIG. S4: **The effect of γ-synchronization on spatial learning**. Each panel represents the results of simulating 150 neuronal ensembles at different effective temperatures $1/\beta$ (colorbar on the right) and different integration times w (scale shown above). Each dot represents a particular ensemble of N_c place cells with the mean place field size s. The maximal firing rates of the simulated neurons are lognormally distributed around $f = 25$ Hz (see Methods in [23, 24]). The color of the dot indicates the average time T_{min} required to encode an accurate map of the environment shown on Figure 2A, averaged over ten place field maps with the same (s, N). If the integration window is large (two left-most columns), γ-synchronization does not produce a strong effect on learning times. As the integration window becomes smaller, cooling the coactivity complex increases the scope of successful place cell ensembles. This implies that that γ-synchronization increases the resilience of the hippocampal network in the face of variations of the place-spiking parameters.

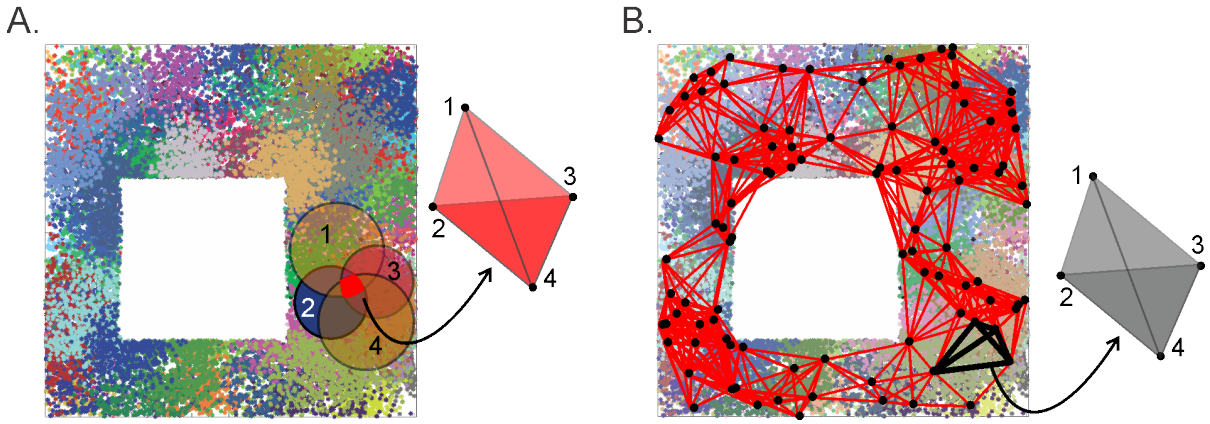

FIG. S5: **The coactivity complexes**. (**A**) Simplexes of the Čech coactivity complex represent simultaneous overlaps of the place fields. (**B**) The place field connectivity graph G: dots represent centers of the place fields, red links represent overlaps between the place fields. The fully connected subgraphs of G (e.g., the six black links at the bottom of the panel) are the cliques of G representing simplexes of the clique coactivity complex $\mathcal{T}_\varsigma$.

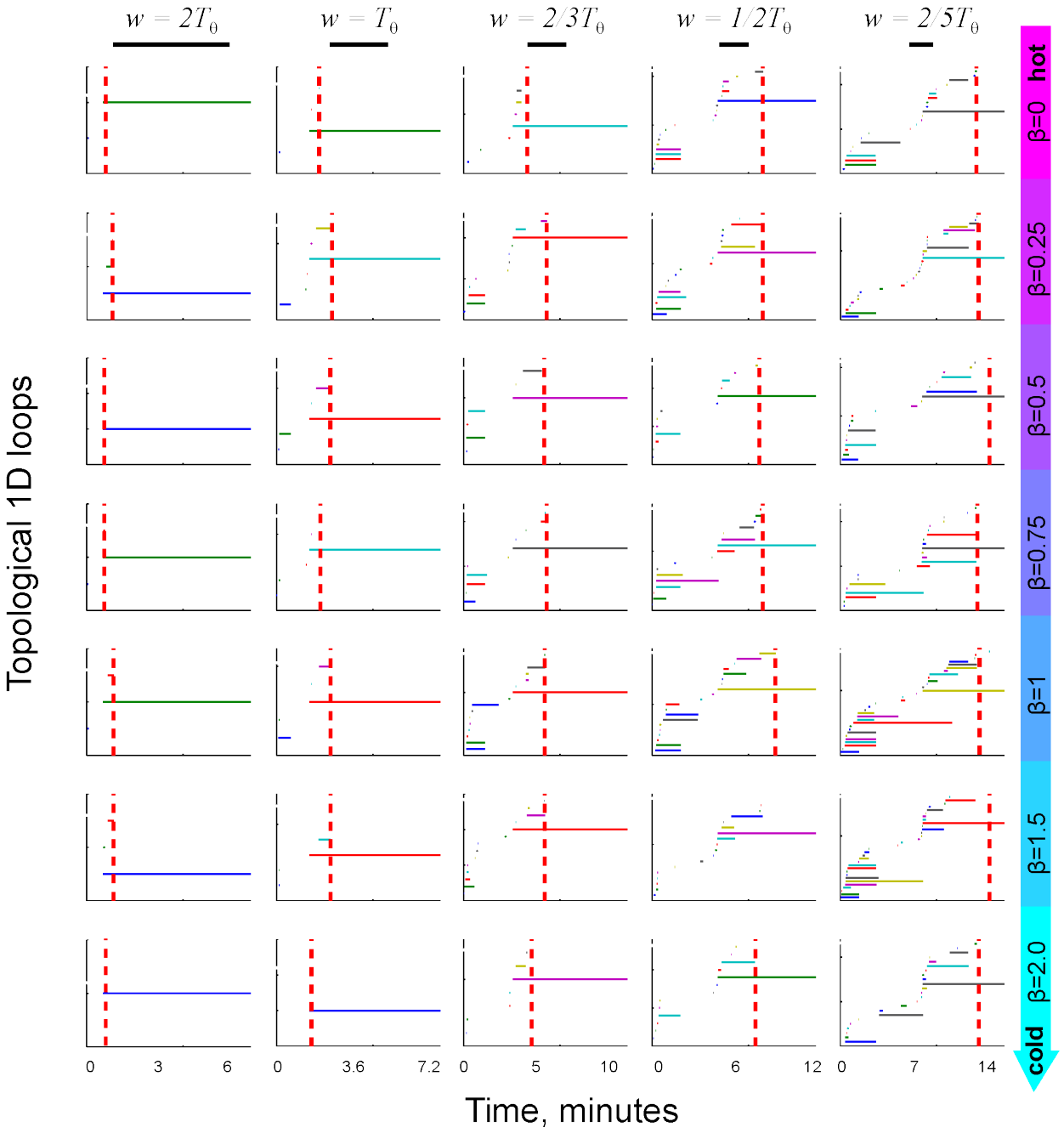

FIG. S6: **Freezing out the spurious loops in clique complex**. Timelines of the topological loops in the clique coactivity complex produced in the environment shown on Figure 1, for different integration windows (scale of ws is shown on top) and different effective temperatures $1/\beta$ (colorbar on the right). The learning times T_{min} are marked by red vertical dashed lines. The qualitative dependence of the number of topological loops in the coactivity complex on the width of the integration window and the effective temperature $1/\beta$ are similar to the ones produced by the coactivity complex. However, the overall numbers of spurious topological loops is smaller, and the coactivity complex has a correct structure even at the smallest integration window $w \approx (2/5)T_\theta$.

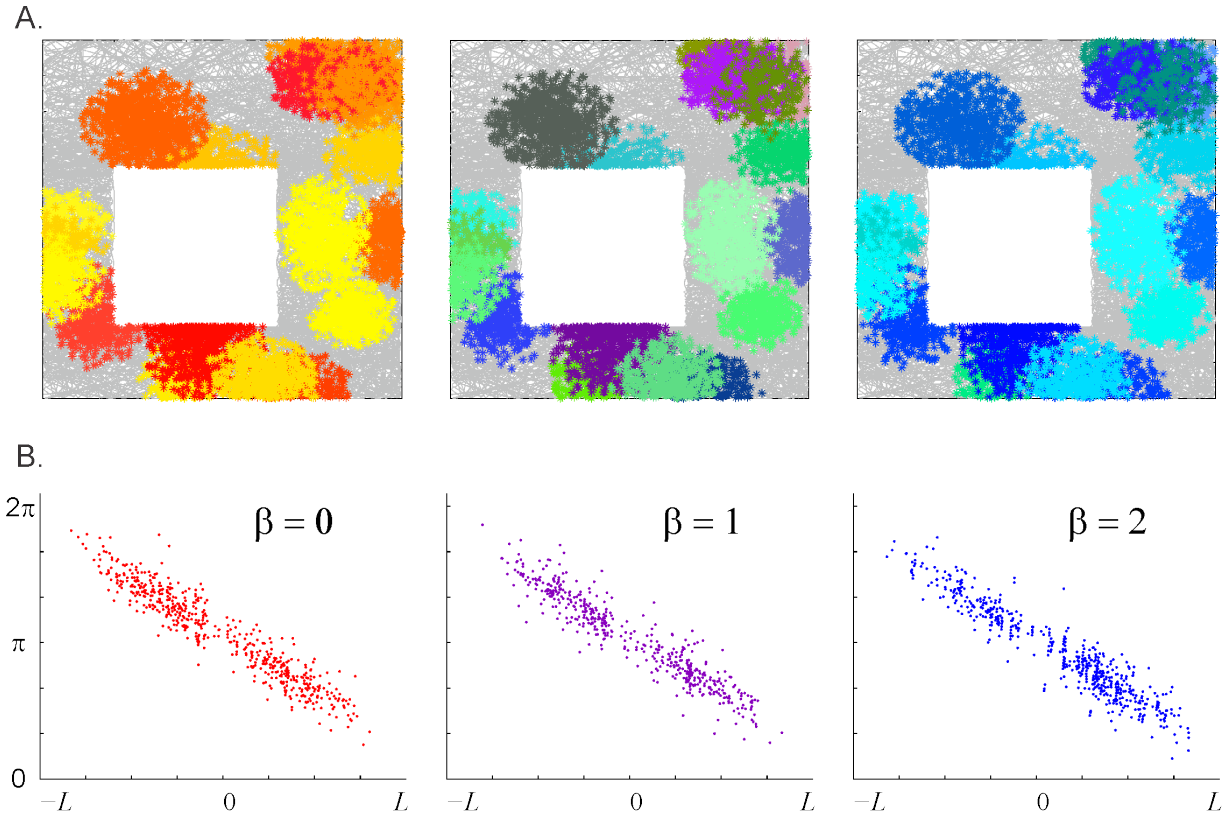

FIG. S7: **Simulated place fields and the θ-precession are not affected by the gamma modulation**. (**A**) Place fields shown for $\beta = 0, \beta = 1$ and $\beta = 2$. (**B**) The θ-phase/position diagram illustrating the θ-precession of a simulated place cell for $\beta = 0, \beta = 1$ and $\beta = 2$.